49th AIAA Aerospace Sciences Meeting including the New Horizons Forum and Aerospace Exposition
4 - 7 January 2011, Orlando, Florida

High Speed and High Reynolds Number Jet Control Using Arc Filament Plasma Actuators for Noise Mitigation and for Flow and Noise Diagnostics

M. Samimy[1], M. Kearney-Fisher[2], J.-H. Kim[3], and A. Sinha[4]
Gas Dynamics and Turbulence Laboratory
Aeronautical and Astronautical Research Laboratories
Department of Mechanical and Aerospace Engineering, The Ohio State University
2300 West Case Road
Columbus, Ohio 43235-7531, USA

We have developed a class of plasma actuators called localized arc filament plasma actuators (LAFPAs) for high-speed and high Reynolds number flow control. Over the past several years, we have successfully used these wide bandwidth (0 to 200 kHz) and individually-controlled actuators to excite the jet shear layer, jet column, and azimuthal instabilities in high subsonic and supersonic jets for either mixing enhancement or noise reduction purpose. In this paper, we provide a brief summary of our work and highlight the capabilities and potential of the actuators and the control technique for not only mixing enhancement and noise mitigation but also for flow and acoustic diagnostics. The jet is operated over a large range of jet Mach numbers (0.9 to 1.65), stagnation temperature ratios (up to 2.5), and Reynolds numbers ($0.2x10^6$ to $1.65x10^6$). Over this entire space of operating conditions, the jet is found to respond to control with a large range of forcing Strouhal numbers and azimuthal modes. The investigations reveal that the jet flow field and acoustic far-field can be dramatically altered, providing a powerful control tool in these practical high-speed and high Reynolds number jets. Sample flow and acoustic results are also presented to demonstrate the capabilities of these actuators and the control technique for flow and acoustic diagnostics.

I. Introduction and Background

Fluid flows are ubiquitous in engineered systems and devices as well as in nature. Over the past several decades, tremendous research effort has gone into the development and implementation of flow control techniques to improve the beneficial effects and/or to reduce the detrimental effects of flows. The nature of the flow control technique used in an application depends on many factors, such as flow type, speed, Reynolds number, cost versus benefit assessment, etc. Numerous flow control techniques have been developed and used over the years to address this broad range of requirements, making a complete categorization quite challenging. Two broad categories of passive and active control have been used in the literature. Passive control almost always involves geometrical modifications, such as vortex generators on a wing of an aircraft for flow separation delay, or chevrons on the exhaust nozzle of an aircraft for noise mitigation. Passive control devices are always 'on' regardless of whether they are needed or the performance penalty that they may incur. Active flow control, on the other hand, involves providing energy or momentum to the flow or the system in a regulated manner, and therefore can be turned 'on' or 'off' as needed. It is clear that active control is more desirable over passive, as it can be turned off when it is not needed to save energy as well as to avert its potential detrimental effects. Since active control is the subject of this paper, it will be further discussed next.

[1]The Howard D. Winbigler Professor of Engineering, AIAA Fellow, corresponding author (samimy.1@osu.edu)
[2] Ph.D. Candidate, AIAA Student Member
[3] Research Associate, AIAA Member
[4] Ph.D. Candidate, AIAA Student Member

I.1. Active flow control

Active flow control is divided into two general categories: open loop and closed loop, or feedback. In the former, the actuation is dictated by an operator based on prior knowledge of the flow. In the latter, there is at least one sensor in the flow to measure the effect of actuation as well as the changes in the flow conditions. At each instant, the measured information is used by either a flow model [1] or an optimization algorithm based on minimal prior knowledge of the flow [2], to prescribe the actuation parameters for the next instant. The focus of this paper is on open loop control, but our jet feedback control using LAFPAs will be briefly discussed later.

Active control can also be classified based on the mechanism of its coupling with the flow. The first category can be called momentum injection or body force use. In this category, for example, the low momentum near-surface flow is energized, as in flow separation control over an airfoil by fluid injection [e.g. 3], or a body force is generated, as by dielectric barrier discharge (DBD) plasma actuators [e.g. 4]. In this momentum injection category, additional (normally streamwise) flow structures are often used, as for noise mitigation using fluidic chevrons [5]. The second category involves excitation of known flow instabilities by providing perturbations of the right frequency and mode. The seeded perturbations are amplified by the flow instabilities and develop into flow structures of the desired characteristics [6]. Indications are that momentum injection and body force type controls have practical limitations in high-speed and high Reynolds number flows due to excessive energy input requirements, whereas such limitations do not seem to exist in control based on instability excitation. A good case in point is the use of traditional DBD actuators (AC-DBD) [7] with limitations in high Reynolds number flow separation control, versus nanosecond pulse driven DBD (NS-DBD) actuators with no such limitations [8-9].

I.2. Jet instabilities and receptivity

Jet instabilities were discussed in detail in Samimy et al. [6, 10]. They will be briefly reviewed here. An axisymmetric jet has two length scales: the initial jet column diameter or the nozzle exit diameter (D), and the initial shear layer or the nozzle exit boundary layer momentum thickness (θ). Detailed instability analyses [e.g. 11] and experimental results [e.g. 12] show that the shear layer is receptive to perturbations over a large range of frequencies ($St_{\theta F} = f_F\theta/U_j \sim 0.01$ to 0.02 where U_j is the jet exit velocity). Maximum growth rate is achieved when the shear layer is forced at $St_{\theta F}$ of around 0.017, and maximum growth occurs in a naturally growing shear layer at St_θ of around 0.012 (note that the 'F' is omitted from the subscript since the variable does not refer to a forced quantity). The jet column is unstable for perturbations over a range of Strouhal numbers ($St_{DF} = f_F D/U_j \sim 0.2$ to 0.6), but the maximum growth of perturbations is obtained when the jet is forced at $St_{DF} \sim 0.3$ [e.g. 13]. For later reference, the Reynolds number for free jets are defined as $Re_D = DU_j/\nu$, where ν is the kinematic viscosity.

In addition to the initial shear layer and the jet column mode instabilities, axisymmetric jets are also susceptive to azimuthal mode instability. The primary parameter affecting the development of azimuthal modes is D/θ [e.g. 14, 15]. Linear stability analysis of Cohen and Wygnanski [15] also showed that for a very thin boundary layer (or very large D/θ), many azimuthal modes are unstable in the initial shear layer region. As will be discussed further later, $D/\theta \sim 250$ in the current research, and the jet is indeed receptive to many forcing azimuthal modes.

The excitation of instabilities in a given flow strongly depends on where the perturbations are introduced, among several other factors. There is a significant body of literature on the receptivity of free shear layers and jets to external perturbations [e.g. 16]. It is generally agreed that: (1) the receptivity is maximum where the shear layer is initiated, namely at the nozzle exit or splitter plate edge; (2) the receptivity is in general better when the perturbations are located upstream rather than downstream of the nozzle exit or splitter plate edge; and (3) jets and free shear layers with laminar initial shear layers are more receptive than those with turbulent initial shear layers. As will be detailed later, the actuators in the current work are located just upstream of the nozzle exit, as close to the maximal receptivity location as possible.

I.3. Various objectives of jet control

Linear stability analysis reported over three decades ago clearly showed that the jet is like a limited band amplifier [e.g. 11]. This finding, along with the visual discovery of large-scale structures in relatively high Reynolds number jets and free shear layers [13, 17], spurred tremendous activities in various aspects of shear layer and jet control over a span of almost 25 years. The objectives of the activities could be loosely divided into noise mitigation, noise amplification, mixing enhancement, and flow diagnostics. These topics will be briefly discussed in the next few paragraphs.

Jet noise mitigation using active control was attempted in the 70's and 80's. However, due to limitations in the excitation amplitude and frequency of the acoustic drivers used for actuation, the investigations focused exclusively on either low Reynolds number ($< 10^5$) jets or moderate Reynolds number jets but with low frequency excitation. In addition, it is not easy to excite azimuthal modes using acoustic drivers, especially in high speed flows. The results in the literature consistently show broadband turbulence amplification as well as far-field noise amplification with pure tone forcing at a Strouhal number around the jet column mode and up to about 1 ($St_{DF} = 0.2$ to 1). The broadband amplification in turbulence and far-field noise was obtained regardless of whether the nozzle exit boundary layer was laminar or turbulent [18-22]. In works using much higher forcing Strouhal numbers ($St_{DF} > 1.5$), the reported results heavily depend on the state of the boundary layer. In low Reynolds number jets with laminar nozzle exit boundary layer, broadband turbulence suppression [12] as well as far-field noise suppression [23-24] were observed with forcing Strouhal number within the jet initial shear layer instability range ($St_{\theta F} \sim 0.012$ to 0.017). When the boundary layer at the nozzle exit was turbulent, Zaman and Hussain [12] observed no effect on broadband turbulence levels, but Moore [19] and Jubelin [25] observed a suppression of 1 to 2 dB in the far-field noise. The broadband suppression or amplification seemed to be almost uniform over the entire frequency range and also over a large range of polar angles with respect to the jet axis.

Aircraft noise is comprised of many components, including noise from fan, compressor, combustor, turbine, jet, and aerodynamics. Jet noise is the dominant component in takeoff and a major component in landing. Each component possesses distinct characteristics that are used to identify it in the acoustic signature of the aircraft. The components have been studied in laboratories and corresponding models have been developed and tested over several decades. However, when these models are used to calculate the noise of various components, including the jet noise, they often significantly under-predict the broadband jet noise from an actual jet engine [19, 26-28]. Understanding of this perplexing issue has challenged researchers for several decades. It was suspected that other noise components, especially those with pure tone components, from the fan, turbine or combustor, were interacting with and exciting the jet, thereby elevating the broadband noise in actual jet engines [20, 29]. To test this hypothesis, researchers introduced pure tone excitation into laboratory jets, and studied their broadband noise amplification characteristics. More detailed information and many references on this topic, as well as on the related research on bulk-mixing enhancement, can be found in Samimy et al. [10].

The use of active jet control as a flow and noise diagnostic aid has paralleled the study of noise amplification/mitigation described above. The three interconnected diagnostic objectives of low-amplitude tone excitation have been: (a) raising the large-scale coherent structures above the background levels, (b) exciting shear layer instabilities, and/or (c) providing a phase reference for measurements. In the seminal work of Crow and Champagne [13] that established the presence of large-scale structures in relatively high Reynolds number jets ($Re \sim 10^5$), the well-defined time-base provided by periodic excitation was used to analyze the data from hot-wire anemometry and schlieren photography. Subsequently, many investigators sought to understand the development, evolution and interaction of such seeded structures, both axisymmetric and helical, using phase-averaged imaging and measurements [e.g. 12, 23, 30-35]. The implication of these discoveries in forced jets for the structure of unforced jets has been debated all along. Crighton [20] and Hussain [36] reviewed various related coherent vortex eduction techniques and discussed some of the relevant issues in the interpretation of such results.

The study of jets with seeded perturbations also has a natural link with stability theory, which predicts the evolution of such perturbations. Several researchers sought to compare and validate

experimental data with theoretical predictions using time-averaged velocity and pressure statistics in the shear layer [e.g. 15, 37-39]. The regularization of the jet structure obtained with low-amplitude excitation has also been of interest in the study of the large-scale structures as noise sources [e.g. 40, 41]. Owing to actuator limitations, most of these efforts were limited to low Reynolds number jets and the axisymmetric forcing mode. One of the few investigations that covered high-speed and high Reynolds number jets and explored some of the above ideas, including non-axisymmetric forcing, was the extensive study performed by the Lockheed Georgia group in 1980's [e.g. 22, 42, and references therein].

I.4. Actuator requirements

Acoustic drivers were used for the majority of shear layer and jet active control in the past with the upper limit of Re_D around 100,000 for most of the work. As the speed and the Reynolds number of the jet increase, so do the background noise, the instability frequencies, and the flow momentum. Therefore, actuators must provide excitation signals of much higher amplitudes and frequencies - two diametrically opposing requirements. As a result, there is practically no work on the active control of high-speed and high Reynolds number jets, with only a few exceptions. For example, Kibens et al. [43] used high amplitude pulsed injection to excite the exhaust from a full-scale jet engine at a mixed or flapping mode ($m = \pm 1$) around the jet column Strouhal number. They used two actuators, operating 180° out of phase and each covering a quarter of the exhaust jet perimeter. This resulted in significantly increased mixing and far field noise radiation. Obviously, the increased scale and thus the reduced frequency (~ 135 Hz) was a key factor in the implementation of actuation in this work. Also, Moore [19], Jubelin [25], Ahuja et al. [44], Lu [27], and Lepicovsky and Brown [45] used acoustic forcing (either channeled the acoustic signal to multiple locations at the proximity of the exit of the jet or used it in the jet settling chamber) to force a high subsonic jet around its column mode. Apart from acoustic drivers, researchers have reported limited use of glow discharge in low Reynolds number jets [30, 40], miniature piezoelectric zero-net-mass-flux devices in a high subsonic jet [46], and arc discharge and laser energy deposition in supersonic jets [35].

We have recently developed a class of plasma actuators, called Localized Arc Filament Plasma Actuators (LAFPAs) that can provide excitation signals of high amplitude and high bandwidth for high-speed and high Reynolds number flow control [6, 47]. The actuators' frequency, phase, and duty cycle can be controlled independently. Therefore, several of these actuators can be used to excite jet column modes, shear layer instability modes, and their various azimuthal modes. In the following sections we will provide a brief background on LAFPAs.

II. Localized Arc Filament Plasma Actuators (LAFPAs) and Control Mechanism(s)

A LAFPA consists of a pair of electrodes, one attached to ground and the other to a voltage source capable of generating high voltage on the order of several kV. An electrically insulating and temperature-resistant annular extension is mounted on the nozzle exit. The 8 LAFPAs used in the current work are distributed uniformly around the nozzle extension perimeter approximately 1 mm upstream of the exit (Figure 1). The distance between the two electrodes in a LAFPA is normally 3 to 4 mm, center-to-center. When the voltage across a pair of electrodes is ramped up to the breakdown voltage (which is several kV and depends on the distance between the electrodes, the air flow properties, and the frequency of operation) the air between the electrodes breaks down and an electric arc is generated. Right after the breakdown, the voltage across the electrodes drops to a few hundred volts and remains at that level until the voltage source is disconnected. The frequency and the duty cycle (the percentage of the period of forcing that the electrodes remain connected to the voltage source) of each actuator are controlled independently by a computer through a PCI board. The frequency and duty cycle can be changed from near zero to 200 kHz and from approximately 3 to 50%, respectively. With the 8 actuators, simple azimuthal modes (m) from 0 to 3 and mixed modes ±1, ±2, and ±4 can be excited by controlling the firing order of the actuators, as briefly explained below. The concept and earlier development of LAFPAs can

be found in Samimy et al. [48], and the latest development and characterizations are given in Utkin et al. [47] and Samimy et al. [6].

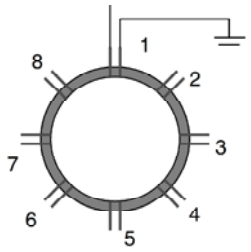

Figure 1: Schematic of the eight LAFPAs distributed azimuthally just upstream of the nozzle extension exit.

In controlling a jet using acoustic drivers, the input signal to the driver is sinusoidal with an amplitude of $A = A_0\sin(2\pi f_F t - m\phi)$ for simple azimuthal modes, where f_F is the forcing frequency, m is the azimuthal mode, and ϕ is the azimuthal location of the actuator. In the plasma actuator, the input signal is a rectangular on/off pulse. It is relatively simple to visualize the input signal. The azimuthal distance between two adjacent actuators is $\pi/4$, as shown in Figure 1. The phase between two actuators fired successively is determined by $\phi = 2m\pi/N$, where m is the azimuthal mode (varies from 0 to 3 with 8 LAFPAs) and N is the number of actuators used, which is 8 in the current work. Therefore, $\phi = 0$ for $m = 0$ mode and all the actuators are operated in phase (at the same time); $\phi = \pi/4$ for $m = 1$ mode and the actuators are operated in sequence, starting with actuator 1 and ending with actuator 8 over one period of forcing; $\phi = \pi/2$ for $m = 2$ mode and the actuators 1&5, 2&6, 3&7, and 4&8 are grouped together and operated in successive order and $\pi/2$ out-of-phase; $\phi = 3\pi/8$ for $m = 3$ mode and the order of actuators operation is 1, 4, 7, 2, 5, 8, 3, and 6. For the mixed mode $m = \pm 1$, the top 3 actuators (8,1,2) and bottom 3 actuators (4,5,6) are operated 180° out of phase and actuators 3 and 7 are inactive.

The duty cycle of the actuators can be varied from approximately 3% to 50%. At the lower end, there may not be sufficient time for breakdown and the actuators could misfire. At the higher end, the resistors in the circuit, used to limit the current, heat up too much and the cooling capacity of the system is not sufficient to handle the heat load. The duty cycle has a significant influence on the effectiveness of control. The optimum duty cycle is found to be the minimum duty cycle just sufficient to produce complete air breakdown between the electrodes [49].

In our earlier work, the electrodes were flush mounted with the inner surface of the nozzle. However, the plasma was noticeably stretched by the momentum of the high-speed flow and eventually swept downstream causing reduction in the effectiveness of the actuation [48]. Therefore, we currently use a circular groove of 1 mm width and 0.5 mm depth, located approximately 1 mm upstream of the nozzle exit, to shelter the plasma. The tips of the electrodes are housed within this groove. In the most recent work, a new nozzle extension was designed, which relocates the electrodes to the nozzle extension face and eliminates the ring groove. The results showed that the effect of the ring groove is secondary and relatively small [49]. In a recent work, Kleinman et al. [50] used direct numerical simulations to investigate the effect of groove on the actuation process in a flow that matches the experimental flow conditions for a Mach 1.3 jet, including the Reynolds number [6]. However, due to the current computational resource limitations, the flow and cavity geometry was restricted to two dimensions, even though the flow within the cavity is clearly three-dimensional. Because of this limitation, the simulation results significantly over-predict the effect of the cavity.

The short duration and harsh high temperature environment of plasma offer a major challenge for any accurate measurements of perturbations imparted to the flow by the actuators. We have used nitrogen emission spectroscopy to measure the average temperature of the plasma, which depends on the frequency and duty cycle of the operation. The temperature, averaged over the spatial extent of the plasma (approximately 1 mm wide and 3 to 4 mm long) and over several pulses, varies from a few hundred to about 1200°C [51]. For example, the measured average temperature with 5 kHz forcing and 15 μs pulse

duration (7.5% duty cycle) is ~1000°C. It appears that a considerable fraction of the discharge power goes to electrode heating. The electrodes used in the current work are tungsten of 1 mm diameter and the nozzle attachment holding the electrodes is boron nitride. Tungsten emission lines, as well as boron nitride and boron oxide bands were detected in the emission spectra, an indication of erosion of electrodes and boron nitride nozzle attachment. Such erosion over time has also been noticed in the experiments. Temperatures measured in our previous work [47] were over-predicted due to the boron oxide emission bands overlapping with the nitrogen bands. These errors have recently been corrected [51].

The jet is known to be receptive to thermal, aerodynamic, and acoustic perturbations [19]. With LAFPAs, the initial perturbation is thermal (i.e. localized Joule heating by the air breakdown). However, the flow is compressible and each actuation causes rapid microsecond time scale localized heating that generates a compression wave [10]. Our earlier unsteady quasi-one-dimensional model of the arc filament showed that the rapid localized heating generated compression waves that were steepened in a short period (~10 μs) and in a short distance (~3 mm) to become a stronger compression wave [47], in general agreement with the experimental results. It is unclear at this time and not possible to discern whether it is the thermal perturbation, the pressure perturbation, or a combination of the two that is coupled to the flow. In addition, our earlier results showed that the actuators could generate streamwise vorticity and vortical/aerodynamic perturbations, the strength of which depends on the distance between the electrodes [48]. However, with 3 or 4 mm distance between the electrodes in the current work, and potentially non-uniform plasma between the electrodes, the generated streamwise vorticity is expected to be quite weak.

A recent numerical simulations work involves large eddy simulation and uses 8 actuators and flow parameters similar to those in the current Mach 1.3 jet experiment, and simulates the effects of actuation as a surface heating [52-53]. The response of the jet to the actuation and the ensuing structures are very similar to those in the experiments, confirming the experimental findings that the ring groove effects are secondary. Another large eddy simulation effort involves details of nozzle geometry and actuators arrangement [54]. It models the plasma as a simple time-varying and spatially-distributed internal energy source, similar to the model used in Utkin et al. [47]. The preliminary results of this work show generation of compression waves by the actuation, similar to those observed experimentally.

III. Experimental Facility and Techniques

A brief description of the experimental facility and techniques utilized in the current work will be given in this section. All the experiments were carried out at the Gas Dynamics and Turbulence Laboratory (GDTL) within the Aeronautical and Astronautical Research Laboratories (AARL) at the Ohio State University. The jet at GDTL is created using compressed air and contoured converging and converging-diverging nozzles of exit diameter D = 2.54 cm (1 in.), designed using the method of characteristics. The air is compressed by three 5-stage reciprocating compressors, filtered, dried, and stored in two cylindrical tanks with a volume of 43 m^3 and pressure up to 16 MPa. The compressed air is supplied to the stagnation chamber of the jet facility, discharged horizontally through the nozzle into an anechoic chamber, and then through an exhaust system to the outdoors (Figure 2).

Currently, the jet facility and the anechoic chamber are being modified. The new jet facility will be capable of using either a 1 in. or a 2 in. jet, and up to 16 actuators. This will enable the usage of azimuthal modes up to 7 to further evaluate the benefits of higher azimuthal modes for noise mitigation. The footprint of the anechoic chamber will be increased by a factor of 2.4, enabling far-field acoustic measurements from 20° to 130° for the assessment of the effect of control on shock noise in supersonic jets.

Far-field sound pressure was measured using a linear array of 1/4 inch B&K 4939 microphones covering 25° to 90° polar angles with respect to the jet axis. The far-field acoustic results are scaled to a distance of 80 jet diameters. The acoustic signal from each microphone is band-pass filtered from 20 Hz to 100 kHz, amplified by B&K Nexus 2690 conditioning amplifiers, and acquired using National Instruments A/D boards and LabView software. The microphones are calibrated using a 114 dB, 1 kHz

pure sinusoidal tone. The frequency response of the microphones is flat up to 80 kHz with the microphone grid cover removed. Blocks of data were collected at 200 kHz with 8192 data points per block, producing a spectral resolution of 24.4 Hz. The sound pressure level spectrum is obtained by averaging 100 blocks of data.

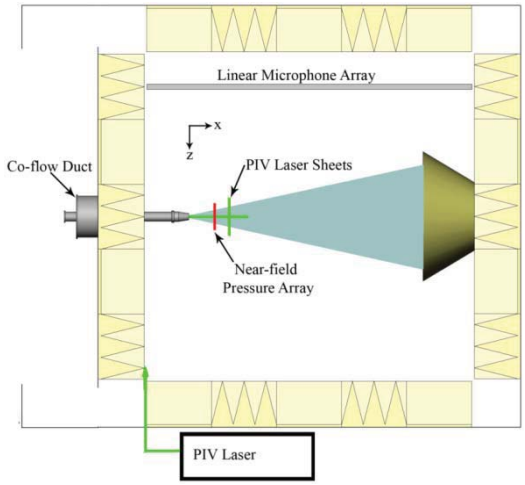

Figure 2. Schematic of jet and anechoic chamber.

A LaVision PIV system with a 2048x2048 pixel resolution camera was used for two-component (streamwise and radial) velocity measurements on a vertical plane passing through the jet centerline. A Spectra Physics Model SP-400 dual head Nd:YAG laser is used as the light source. The cameras and laser are synchronized by a timing unit housed in a dual processor PC. The spatial resolution of the velocity vectors depends on the field of view, and the number of pixels used. For most of the streamwise velocity field measurements, the spatial resolution is about 2.2 mm. The laser sheet thickness is less than 0.3 mm. The time separation between two consecutive PIV images ranged from 1.8 to 4 μs (depending on jet exit velocity) so the velocity field from a pair of PIV images is almost instantaneous. In initial processing, an interrogation window of 64x64 pixels was used. Then this reduced data was used as a reference in final processing with an interrogation window of 32x32 pixels with 50% overlap to increase spatial resolution of the computed vector fields. PIV data are collected as 700 statistically random snapshots. Turbulence statistics were obtained using 700 image pairs; convergence of statistics was achieved with 600 to 650 image pairs. Phase-averaged flow-fields are constructed by conditional-averaging of the random data set computed as a post-processing step. More information on this process can be found in [55-56].

The jet plume was seeded with liquid droplets atomized by a four-jet LaVision atomizer in unheated jets. For heated jets, aluminum oxide particulates suspended in ethanol were used [55]. A 38.1 cm duct, made of 1 mm thick sheet metal, was placed around the jet to generate a very low-speed co-flow (see Figure 2). The co-flow velocity was less than 3 m/s (less than 1% of the jet exit velocity). The co-flow was generated by allowing a significant portion of the ambient air entrained into the jet to pass through the duct. The co-flow was seeded by a Concept Model ViCount Compact 1300 fogger to avoid statistical bias in the measurements, as well as the computation of spurious velocity vectors in the entrained air that had not yet mixed with the jet. The average droplet size was about 0.7 and 0.25 μm for the jet flow and co-flow, respectively. The solid particles have a mean diameter of 0.6 μm.

Schlieren images of the jet were collected using a Z-type schlieren system. The system uses a Palflash 501 High Intensity Illumination Flash unit with a flash duration of approximately 500 ns, which is short enough to create a quasi-frozen flow field during imaging. Phase-locking the schlieren images allows for observation of details of flow and wave structures.

IV. Experimental Results

Over the past several years, we have carried out detailed experiments to investigate the effects of LAFPAs on both the flow field and far-field acoustics of unheated and heated Mach 0.9, 1.3, and 1.65 jets [6, 55, 57-62]. For the Mach 1.65 jet, two nozzles were used; a standard contoured nozzle designed using the Method of Characteristics, and a conical nozzle (both conical converging and diverging sections, with a sharp throat) typical of the variable area nozzles used in tactical aircraft. The ratio of the stagnation temperature of the jet to the room temperature (*TTR*) varied from 1 to 2.5, and Re_D varied from approximately $2\text{x}10^5$ to $1.7\text{x}10^6$. We have also carried out limited reduced-order model development and feedback control work using a Mach 0.9 jet [2, 63]. Only some selected results will be presented and discussed below.

IV.1. Boundary layer at the nozzle exit

It has been known that the state of the boundary layer at the nozzle exit plays a significant role in the response of the jet to excitation and also in the initial development of structures in the shear layer of the jet. The 2.54 cm (1 in.) inner diameter axisymmetric nozzles with a design Mach numbers of 0.9, 1.3, and 1.65 (except for the 1.65 conical nozzle) all have smooth and gentle converging and diverging sections. In addition, a 2.54 cm inner diameter nozzle extension with a length of 1.9 cm (0.75 in.), which is attached to the nozzle to house the actuators, provides relaxation to the boundary layer developed within the nozzle. There is also a 1 mm wide and 0.5 mm deep ring groove in the nozzle extension about 1 mm upstream of the exit to shelter the plasma. With a high Reynolds number, a gentle expansion of the flow within the nozzle, and relaxation within the nozzle attachment, the boundary layer is expected to be turbulent. However, the boundary layer thickness is estimated to be on the order of 1 mm, which makes it nearly impossible to make measurements at a sufficient number of points within the boundary layer to determine its characteristics.

We recently used a 3.8 cm (1.5 in.) converging nozzle attached to the current jet facility and a hot-wire to make measurements within the initial shear layer of an unheated subsonic jet, approximately 2 mm downstream of the nozzle exit [55]. We limited the Mach number from 0.25 to 0.65, and Reynolds number approximately from $2\text{x}10^5$ to $6\text{x}10^5$, to avoid significant density variations and complications with hot-wire measurements. When the nozzle extension was attached, all the normalized profiles for various Mach number and Reynolds number jets were collapsed, thereby indicating turbulent flow over the range of Reynolds numbers tested. Note that $2\text{x}10^5$ is the lowest Reynolds number (for Mach 0.9 and temperature ratio of 2.5) used in the current jet experiments. The effects of the nozzle extension with or without the ring groove were similar. On the other hand, without the nozzle extension for the boundary layer relaxation, the profiles did not collapse, indicating either a laminar or transitional boundary layer. These results confirm that the boundary layer at the nozzle extension exit in the current work is turbulent.

Fitting a hyperbolic tangent curve to the velocity profiles and employing a technique used by Bechert and Stahl [64], the boundary layer thickness and momentum thickness were respectively determined to be ~1.2 mm and 0.1 mm at the higher end of the Reynolds numbers [55]. Therefore, the best guess at this time is that the boundary layer thickness and momentum thickness in the current work are on the order of 1 mm and 0.1 mm, respectively.

IV.2. Effects of control on the flow structures

The effects of excitation using LAFPAs on the jet flow structures have been explored over a wide range of Mach numbers and temperatures. Table I shows the jet important variables for the cases discussed in this paper, including the jet Mach number (M_j), acoustic Mach number (M_a), and theoretical convective Mach number (M_c), as well as the stagnation temperature ratio (*TTR*) and Reynolds number based on the jet diameter (Re_D). There is a myriad of publications in the literature on the identification of structures in a flow [e.g. 65-68]. The three methods that we have found quite useful with the two-component PIV data are the techniques based on the Galilean streamlines [68], swirling strength [67], and

Q-criterion [65]. Combining the first one with one of the other two provides even better visualization of the structures in the high Reynolds number flows of interest in the current work.

Table I: Important jet parameters.

M_j	TTR	M_a	M_c	Re_D x 10^{-6}
0.9	1.0	0.83	0.43	0.61
	1.5	1.02	0.47	0.36
	2.0	1.18	0.50	0.26
	2.5	1.32	0.53	0.20
1.3	1.0	1.12	0.60	1.07
	1.5	1.38	0.66	0.63
	2.0	1.59	0.71	0.44
	2.5	1.78	0.74	0.34
1.65	1.0	1.33	0.73	1.65
	1.5	1.63	0.81	0.96
	2.0	1.88	0.87	0.67
	2.5	2.1	0.92	0.51

Figure 3 shows superimposed phase-averaged Galilean streamlines and normalized Q-criterion for an excited Mach 0.9 jet with a Reynolds number of about 0.61×10^6. The excitation is around the jet column frequency ($St_{DF} = 0.33$) and the two excited azimuthal modes are: (a) axisymmetric mode ($m = 0$) and (b) flapping mode ($m = \pm 1$). For the Galilean streamlines, the coordinate system is convecting with the large-scale structures. If there are relatively coherent large-scale structures in the flow and if the convective velocity used in the calculation remains relatively constant, the structures are identified by streamlines spiraled around the core of the structures or by closed streamlines, as shown in Figure 3. The convective velocities used in the calculation of the Galilean streamlines are computed from the data using spatial-correlations of the Q-criterion fields. The spatial-correlations produce the structure spacing (λ) and the convective velocity is calculated as $U_c = \lambda f$ where f is the forcing frequency. This procedure is explained in more detail in [69].

The Q-criterion (equation 1) separates the anti-symmetric (rate of rotation), $\mathbf{\Omega}$, and the symmetric (rate of strain), $\mathbf{S}$, components of the velocity gradient tensor, and therefore it identifies the core (positive Q) and the braid (negative Q) regions of the structures in the flow, as shown in Figure 3.

$$Q = \frac{1}{2}(\|\mathbf{\Omega}\|^2 - \|\mathbf{S}\|^2) \qquad (1)$$

Note that the Q-criterion shown in the figures is normalized by $(D/U_j)^2$. Coherent structures are identified with both azimuthal mode of excitation cases. These structures grow in size and strength up to about $3D$ to $4D$, followed by weakening and eventual disappearance, either due to their interaction and disintegration, or by developing jitter, and thus getting smeared out in the phase-averaging process. The main difference between the two excited azimuthal mode cases is in the arrangement of the structures – symmetric with respect to the jet axis in the $m = 0$ and anti-symmetric in the $m = \pm 1$ cases. These two very different structure identification techniques agree quite well in identifying the structures and marking their core and braid regions.

Excitation around the jet column frequency with $m = 1$ (not shown) generates large-scale structures similar to those shown in Figure 3. However, with higher azimuthal modes of excitation, identification of the structures on a planar view becomes much more challenging. Recent numerical simulation results [52-53] show details of these structures in three dimensions and reveal intricacies of their evolution, interactions, and disintegration.

The effects of variations in the jet Mach number and temperature on the jet excitation are shown in Figure 4. For all the cases shown, the forcing azimuthal mode and Strouhal number were kept at $m = \pm 1$ and $St_{DF} = 0.33$. Surprisingly, with the tremendous changes in the Reynolds number (0.26×10^6 to 1.65×10^6), convective Mach number (0.43 to 0.73), and acoustic Mach number (0.83 to 1.59), the

response of the jet to the excitation seems to be quite similar and there are no major changes in the nature of the developed large-scale structures. The conclusion is similar in other excitation azimuthal modes and Strouhal numbers.

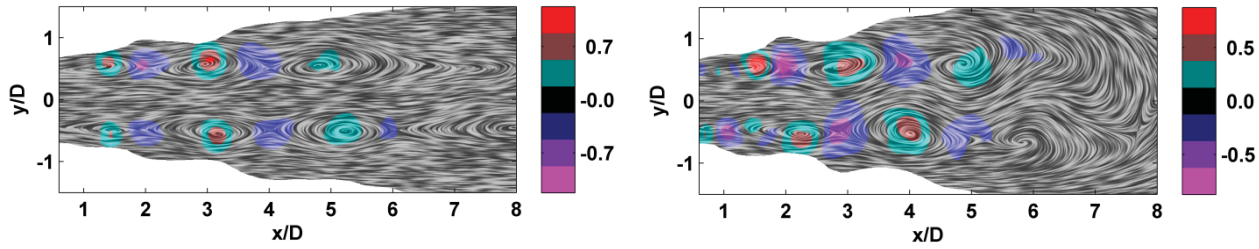

(a) $m = 0$ (b) $m = \pm 1$

Figure 3: Superimposed phase-averaged normalized *Q*-criterion and Galilean streamlines for Mach 0.9 unheated jet excited at St_{DF} = 0.33 and (a) axisymmetric azimuthal mode (m = 0) and (b) first flapping mode (m = ±1).

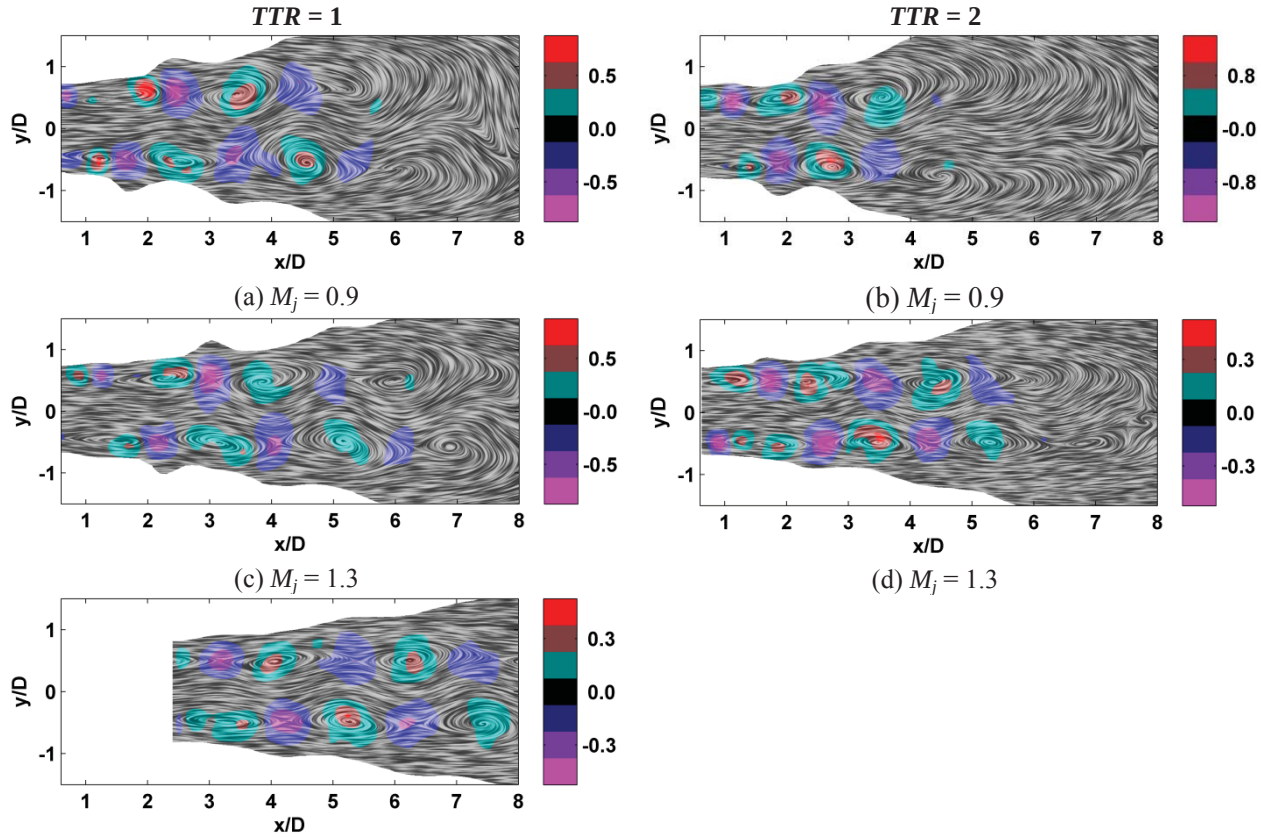

(a) $M_j = 0.9$ (b) $M_j = 0.9$

(c) $M_j = 1.3$ (d) $M_j = 1.3$

(e) $M_j = 1.65$

Figure 4: The effects of excitation on flow structures at various jet Mach numbers and temperatures: m = ±1 and St_{DF} = 0.33, unheated jet on the left column and stagnation temperature ratio (*TTR*) = 2 jet on the right column.

It is clear from the results presented in Figures 3 and 4 that the jet responds in a similar fashion to excitation around the jet column Strouhal number regardless of the jet Mach number, temperature, or the excitation azimuthal mode. The effect of excitation Strouhal number at $m = \pm 1$ is shown in Figure 5 for the unheated M_j = 1.3 jet. Increasing the St_{DF} from 0.33 to 0.52 reduces the size and spacing of the

structures, as expected, but the structures remain coherent until x/D ~7, just downstream of the end of potential core, similar to those at the lower St_{DF}. At the higher St_{DF} of 1.05, the structures are still coherent and quite discernible, though much smaller, in the early part of the shear layer (up to x/D ~ 4), but they either disintegrate or develop significant jitter and get smeared out in the phase averaging process further downstream. This behavior of the structures is reflected also in the jet overall growth, in that the jet grows continuously even downstream of the end of the potential core when excited at lower St_{DF}'s, but it grows much faster up to x/D ~ 4, and then saturates at higher St_{DF}'s [10].

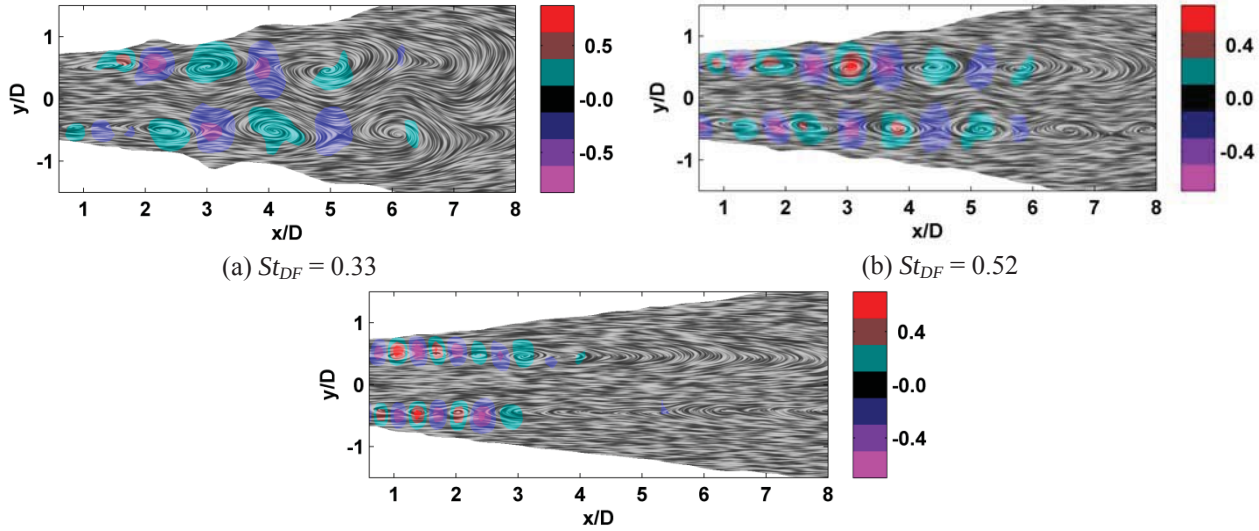

(a) St_{DF} = 0.33 (b) St_{DF} = 0.52

(c) St_{DF} = 1.05

Figure 5: The effects of forcing Strouhal number on flow structures: M_j = 1.3, TTR = 1, and m = ±1.

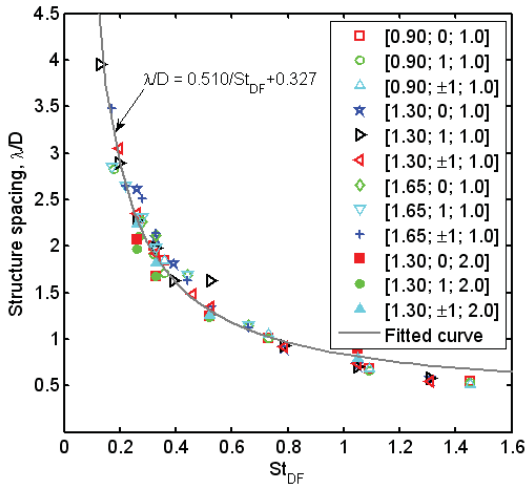

Figure 6: The effects of St_{DF} on structure spacing for various jet Mach numbers, temperatures, and forcing azimuthal modes: the order of numbers in the legend is M_j, m, and TTR.

Only sample results of the excitation effects on the flow structures are shown in Figures 3 to 5. Spatial-correlation of PIV images were used to determine structure spacing in three jets with two different temperatures listed in Table I for various St_{DF}'s and m's. Either the radial component of velocity [59] or Q-criterion [61] were utilized to determine the structure spacing. The results shown in Figure 6 more

quantitatively illustrate the similar response of the jet to excitation regardless of the jet Mach number or temperature covering a large range of jet convective and acoustic Mach numbers. All the results collapse well on a single curve of equation

$$\frac{\lambda}{D} = \frac{0.51}{St_{DF}} + 0.33 \quad (2)$$

where λ is the structure spacing.

IV.3. The effect of excitation on far-field acoustics

The results presented in Figures 3-6 clearly demonstrate that over a large range of Mach numbers, temperatures, and Reynolds numbers, the jet responds to excitations of various azimuthal modes and Strouhal numbers. Additionally, excitation can significantly alter not only the nature but also dynamics of large-scale flow structures. It is noteworthy that the actuation provides perturbations with selected frequency and mode, and the flow instabilities amplify them. These amplified perturbations roll-up into large-scale structures. It has been known for quite some time in the literature that the dynamics of these large-scale structures are responsible for the peak noise in the shallow angles with respect to the jet axis. Therefore, these actuators can be used as a tool to tailor the flow structures, and thus the far-field radiated noise. It should also be mentioned that we do not have direct control on small-scale flow structures, which are a by-product of the interaction and disintegration of large-scale structures. The dynamics of these structures generate noise that primarily radiates to the sidelines (around 90°). Sample far-field acoustic results showing the effects of actuation on the far-field acoustics will be presented and discussed in this section.

The two main effects of the control on the far-field acoustics are the appearance of the actuation tone and its harmonics, and the change in the broadband shape and level. Both of these heavily depend on the polar angle as well as on the forcing Strouhal number and azimuthal mode. Figure 7 shows far-field spectra at two polar angles of 30° and 90° for Mach 1.3 jet at two temperatures: unheated and moderately heated jets with *TTR* = 1.0 and 2.0, respectively. The general trend of the effects of simple azimuthal modes (m = 0, 1, 2, 3) is that m = 3 provides maximum reduction in the peak noise around 30° polar angle (as well as maximum reduction in *OASPL*). On the other hand, m = 0 provides maximum amplification around 90°, though at a lower St_{DF}. The four St_{DF}'s selected for Figure 7 are chosen as follows: the top two are those for maximum noise reduction with m = 3 at 30° at the two temperature ratios (as indicated), and the bottom two are for maximum noise amplification with m = 0 at 90° at the two temperature ratios (as indicated). The following observations regarding the excitation tones can be made from the results shown in Figure 7 and others not shown here: (1) the tone amplitude increases with the temperature; (2) the tone amplitude is much lower with m = 3 than m = 0; (3) the tone amplitude at 90° is much lower than that in 30°. Preliminary results in a much larger facility showed much diminished tone amplitude in comparison with the broadband noise amplitude [70]. More work on this issue is forthcoming. Regarding the broadband noise amplitude, both noise reduction and amplification level are increased with temperature. The effects of actuation on broadband noise will be further discussed next.

Figure 8 shows the effect of St_{DF} on the $\Delta OASPL$ (= $OASPL_{forced}$ - $OASPL_{baseline}$) for a Mach 1.3 jet at *TTR* of 1.0 and 2.0, and for m = 0 and 3 over polar angles of 25° to 90°. In both temperature ratio cases, higher St_{DF}'s reduce broadband noise over all polar angles and lower St_{DF}'s increase it over all polar angles, except at *TTR* = 2 at shallow polar angles, especially for m = 3 excitation. The effect of actuation is improved at the higher *TTR*, especially for m = 3 excitation at shallow angles and lower St_{DF}'s. While there is no Mach wave radiation in the unheated Mach 1.3 jet with M_a = 1.12 and M_c = 0.6 (see Table I), it is significant in the heated jet of *TTR* = 2 with M_a = 1.59, and M_c = 0.71 [69]. Mach wave radiation changes the nature of far-field noise, which includes a shift to higher polar angles of the peak noise.

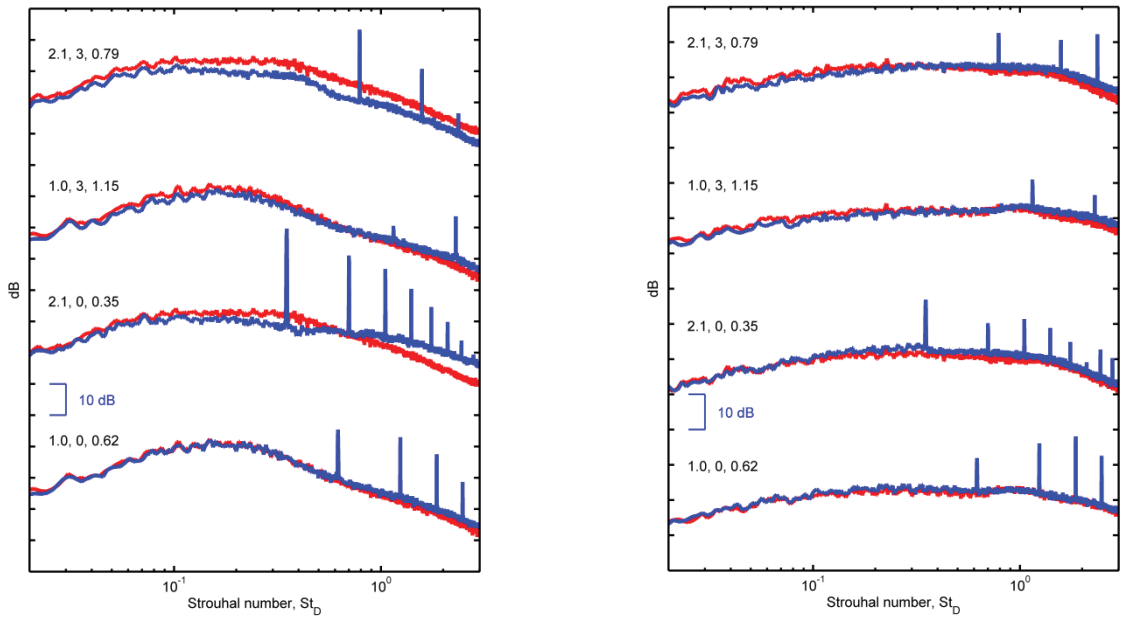

(a) 30˚ polar angle (b) 90˚ polar angle

Figure 7: Far-field acoustic spectra for Mach 1.3 jet showing actuation tones and their harmonics: the numbers next to the spectra are *TTR*, *m*, and St_{DF}. The blue forced spectra and the corresponding red unforced spectra are overlaid.

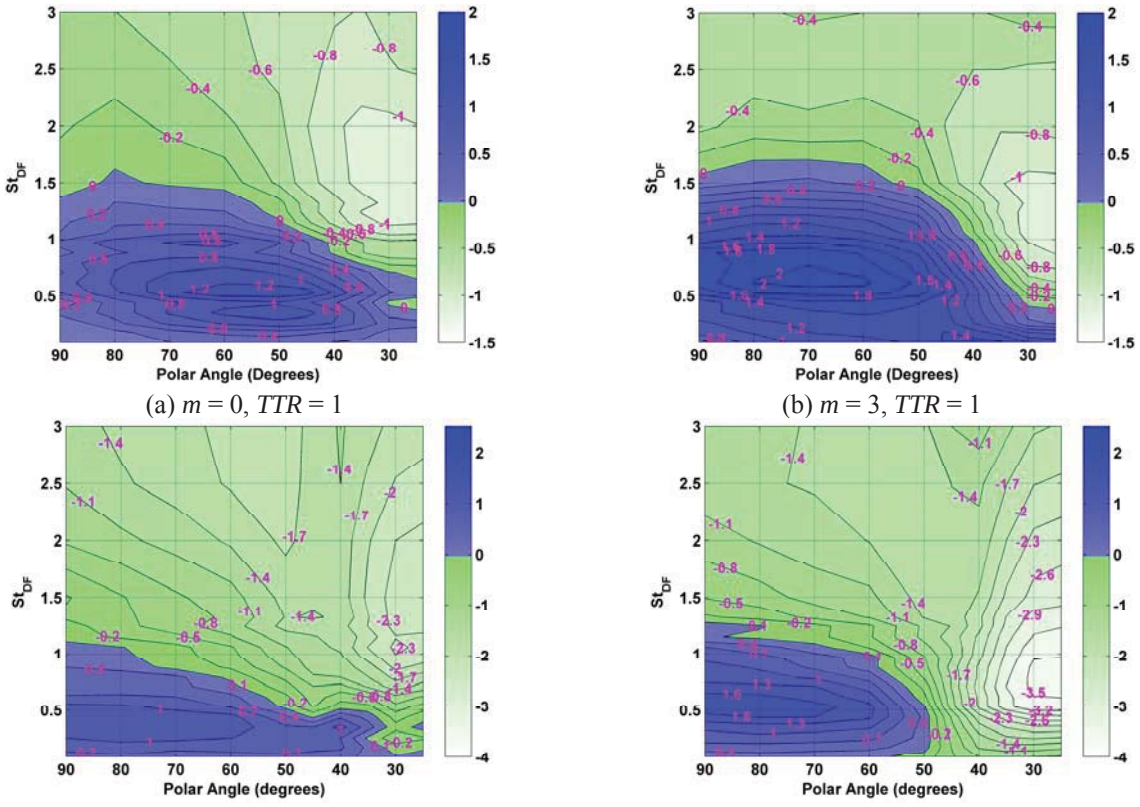

(a) $m = 0$, $TTR = 1$ (b) $m = 3$, $TTR = 1$

(c) $m = 0$, $TTR = 2$ (d) $m = 3$, $TTR = 2$

Figure 8: The effects of St_{DF} on $\Delta OASPL$ in the Mach 1.3 jet at $m = 0$ and 3 and $TTR = 1$ and 2.

Based on the results presented in Figure 8 and other similar results, Figure 9 is generated which shows the effects of jet Mach number and temperature on the maximum noise reduction at 30° polar angle with $m = 3$ excitation, and on the maximum noise amplification at 90° polar angle with $m = 0$ excitation. There is a clear temperature effect in the Mach 0.9 and 1.3 jets with significantly higher noise reduction at higher temperatures. However, the temperature does not have a clear effect on noise reduction in Mach 1.65. Raising Mach number and/or temperature moves the jet into the Mach wave radiation regime and changes the far-field noise characteristics. Mach wave radiation starts around $TTR \sim 2.5$ in Mach 0.9 jet, but it is relatively strong at higher TTR's in Mach 1.3 and even in unheated Mach 1.65 [69]. In addition, compressibility effect is relatively minor in Mach 0.9 jet even at $TTR = 2.5$ ($M_c = 0.53$), but quite strong in Mach 1.3 jet ($M_c = 0.71$ with $TTR = 2.0$) and in Mach 1.65 jet ($M_c = 0.73$ at $TTR = 1$). Currently, we do not have sufficient knowledge of the effects of Mach wave radiation or compressibility on the actuation authority.

Noise amplification at the sideline (Figure 9) is not a desirable outcome but a by-product of manipulation of large-scale structures by actuation. As was shown in Figure 8, lower St_{DF}'s amplify noise over a large range of polar angles, especially at the sideline. There does not seem to be any trend in the temperature effect, however, there seems to be a Mach number effect with much higher amplification in lower Mach numbers. Since this is a by-product of manipulation of large-scale structures by actuation, it is much harder to understand the effects of Mach wave radiation, compressibility, and other variables on noise amplification. Perturbation levels that are much higher than is needed could be one possible explanation of the much higher noise amplification in the Mach 0.9 jet. We do not have direct control on the perturbation level provided by the actuators, and therefore, it is possible that 8 actuators is excessive, but they are needed to force the higher azimuthal modes. Further investigation of this issue is forthcoming.

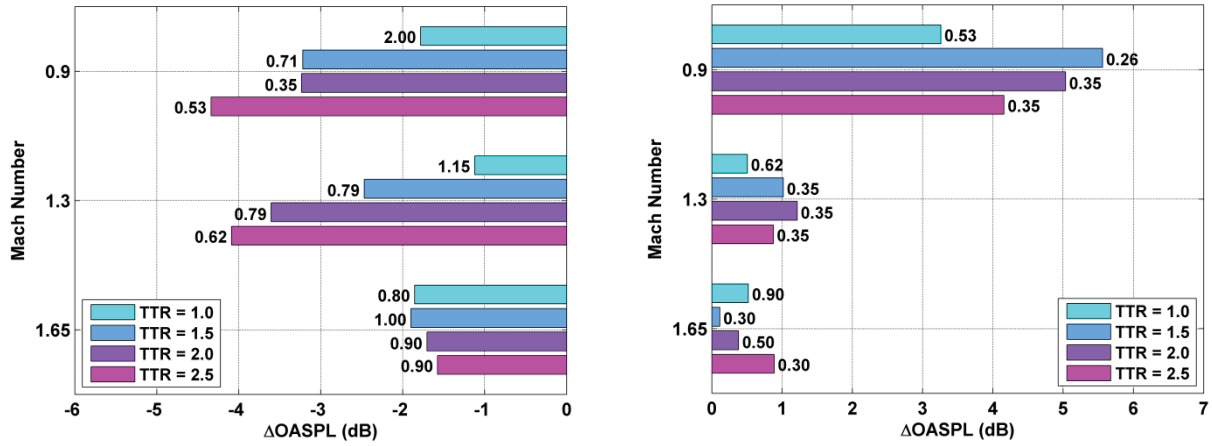

(a) $m = 3$, 30° polar angle (b) $m = 0$, 90° polar angle

Figure 9: (a) Maximum far-field acoustic reduction at 30° polar angle with $m = 3$ excitation, and (b) maximum noise amplification at 90° polar angle with $m = 0$ excitation, at several jet Mach numbers and temperatures.

IV.4. Near-field pressure measurements for feedback control

A limited investigation has been performed on the pressure field in the irrotational region of the jet with the goal of incorporating its real-time sensing in a feedback control loop [2, 10]. Earlier researchers had reported on the strong correlation between the velocity fluctuations associated with large-scale structures in the shear layer and near-field pressure fluctuations [71-73]. Since the LAFPAs are shown to affect these larger-scale structures, it was hypothesized that a real-time estimate of this effect may be sensed in the near-field pressure. Moreover, the axisymmetric mode of the near-field pressure has also been found to be strongly correlated with the intensity of the mixing noise radiated to the far-field [74-

76]. With this in mind, an azimuthal array of pressure sensors was developed and implemented in a simplistic feedback loop to determine the forcing parameters in real-time that either (a) minimized fluctuations in the axisymmetric mode of pressure, or (b) maximized fluctuations in the sum of the axisymmetric and first helical modes [2]. Achievement of the first goal was indeed found to correspond to the forcing parameters converging upon the optimal values found in open-loop parameter sweeps as reported in Figures 8 and 9. The spectrum of the far-field pressure during steady-state operation of the controller also indicated this convergence. Imposition of the second objective was found to drive the forcing frequency to the jet column mode, which is optimal for bulk mixing enhancement.

The simplistic feedback controller described above suffers from a slow rate of response compared to the time-scales of the flow. To obtain faster controllability, one needs to develop a reduced-order model of the velocity field, along with a dynamic estimator and sophisticated control algorithms. This work is ongoing and progress in this direction has been reported in [63, 77].

IV.5. Control employed as a tool for flow and noise diagnostics

The results to date have shown that LAFPAs have the ability to manipulate jets over a wide range of Mach numbers and temperatures. However, the existing body of research with LAFPAs has been focused on specific applications for such manipulation (i.e. demonstrating the capabilities for mixing enhancement or noise control). While LAFPAs show great promise for these specific applications, the utility of LAFPAs as a diagnostic tool should not be overlooked.

The uses for LAFPAs as a diagnostic tool stem from two related effects: (1) the creation of a well-defined spatiotemporal origin for large-scale structures, and (2) the regularization of large-scale structure development. It should be obvious that these characteristics are similar to those provided by other active control techniques (e.g. acoustic drivers, pulsed microjets, etc.). The distinguishing characteristic of LAFPAs is their effectiveness at high Reynolds number ($Re_D \sim 10^6$ or higher) and high bandwidth ($f \sim$ 100 kHz) regimes where none of the other active control techniques have been effective. The turbulence in this high *Re* regime complicates analysis of the dynamic governing processes like noise production and vortex development/interaction. In short, LAFPAs can potentially do for the understanding of these high Reynolds number jets what acoustic drivers did for the understanding of lower Reynolds number flows by providing control authority in this regime.

Each individual LAFPA produces a perturbation which grows and gives rise to a structure when the frequency and mode of actuation fall within the range of unstable variables in the flow. Depending on the firing parameters, the structures from individual LAFPAs may or may not merge into a cohesive structure (such as a ring vortex or helix). From the perspective of using LAFPAs as a diagnostic tool, the most important aspect of this forcing mechanism is that the time and location of perturbations that give rise to individual structures is quite narrowly defined. While the positional uncertainty of this origin is on the order of the electrode spacing (~1 mm), the results to date indicate that the temporal uncertainty is quite low (~20 ns). The high degree of temporal localization is based on the conclusion that the voltage breakdown process (which takes about 10-20 ns) is responsible for the control authority of LAFPAs. In contrast, determining the temporal origin for a structure produced by pure tone acoustic excitation to sub-period accuracy is quite difficult due to the smooth nature of a sinusoidal signal.

The high degree of localization in the spatiotemporal position of the perturbation opens areas of study which would be otherwise inaccessible. Pure tone excitation gave researchers the ability to localize events in terms of phase angle. LAFPAs, however, can provide a complete time history. Stability analysis shows that, under the appropriate conditions, a perturbation will roll up into a structure, but the very beginnings of this roll-up process are impossible to observe unless one knows exactly where and when to look. However, by creating a well-defined spatiotemporal origin, LAFPAs provide a means of examining the growth and evolution of structures with a high degree of fidelity – limited by the other diagnostic tools being used in conjunction with LAFPAs. With the appropriate experimental equipment (or simulation parameters), the life of a single structure can be examined from beginning to end. This experimental capability, as might be expected, can also be used to perform analyses similar to those done

with other flow control techniques (phase-locking, conditional averaging, etc.). For example, phase-averaging was employed in the calculation of *Q*-criterion and Galilean streamlines shown in Figures 3-5.

Another consequence of active control is the regularization of certain flow characteristics. The artificial perturbations have repeatable parameters which result in large-scale structures with more repeatable characteristics. As is seen in other control techniques, the large-scale structure growth rates, convective velocities, rotational energies, etc. are all regularized by forcing. This offers obvious benefits in the form of potential for examining these quantities in jets at different operating conditions with enhanced repeatability. This consequence of forcing also has implications for acoustics studies. As reported by Kastner et al. [60], forcing has the effect of concentrating certain types of noise events into a smaller spatial region around the end of the jet potential core. With noise production events confined to a smaller domain, other diagnostic tools can be focused onto a smaller region – increasing the ability to examine the dynamics surrounding jet noise production. As an example: with the use of a hydrodynamic pressure measurement array and a near-field acoustic array, time resolved measurements of pressure fluctuations associated with the flow-field can be related to the time-resolved measurements of an outgoing acoustic wave. While this can be tried in an unforced jet, the relatively predictable location and time of flight of a structure can radically improve the ability to interpret the results.

As an example of the diagnostic capabilities of LAFPAs, they were used in a recent study of Mach wave radiation over the range of jet Mach numbers and temperatures shown in Table I [69]. Figure 10 shows two phase-averaged schlieren images of the Mach 1.3 jet with $TTR = 1.75$ ($M_a = 1.49$) and Mach 1.65 jet with $TTR = 2.5$ ($M_a = 2.1$), both excited with $m = 0$ and $St_{DF} = 0.6$. The main observations from these images are: (1) compression waves in the irrotational field coalesce to form the Mach waves; (2) Mach waves are curved at lower M_a's and become flat at higher M_a's; (3) the radiation angle also changes with M_a. While the last observation is known in the literature, the other observations (the nature of formation and the change in the Mach wavefront shape) are made possible by the excitation.

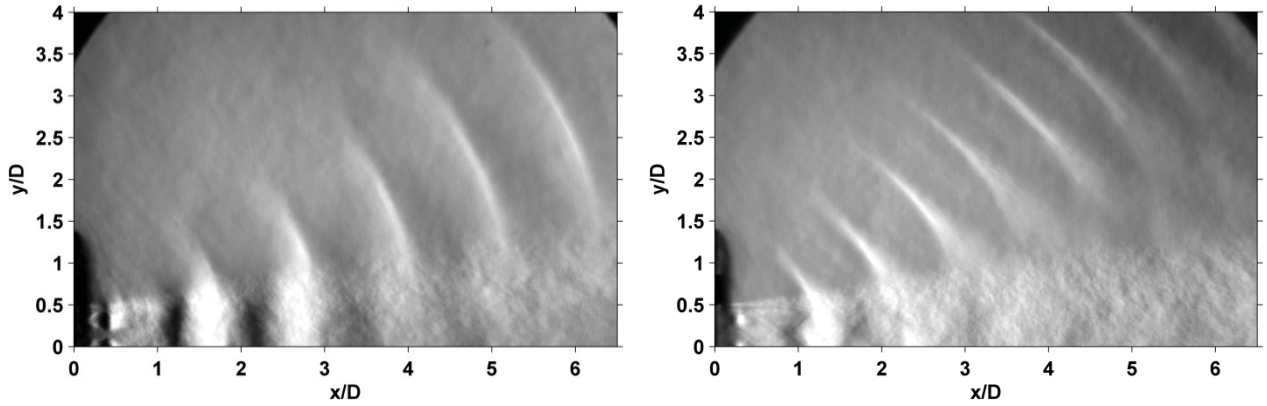

(a) $M_j = 1.3$, $TTR = 1.75$ (b) $M_j = 1.65$, $TTR = 2.5$

Figure 10: Phase-averaged schlieren images of Mach 1.3 and 1.65 jets of different temperatures excited with $m = 0$ and $St_{DF} = 0.6$.

V. Concluding Remarks

In this paper, we have provided a brief overview of our work on the development of a class of plasma actuators called localized arc filament plasma actuators (LAFPAs) for high-speed and high Reynolds number flow control. Over the past several years, we have successfully used LAFPAs to excite various instabilities in high subsonic and supersonic jets with a focus on either mixing enhancement or noise reduction. We distribute 8 of these wide-bandwidth (0 - 200 kHz) actuators just upstream of the exit of the nozzle, close to the receptivity location of the jet shear layer. With individual control of the actuators, we can excite jet shear layer instability, jet column instability, and various jet azimuthal

instabilities (m = 0, 1, 2, 3, ±1, ±2, and ±4). The primary control mechanism is localized Joule heating, which results in the generation of compression waves. It is not clear whether the heating itself, the compression waves, or a combination of the two couple to the flow.

In this paper, we provide a brief summary of our work and highlight the capabilities and potential of the actuators and the control technique for not only mixing enhancement and noise mitigation but also flow and acoustic diagnostics. The results show that the jet, when operated over a large range of jet Mach numbers (0.9 to 1.65), stagnation temperature ratios (up to 2.5), and Reynolds numbers (0.2×10^6 to 1.65×10^6), responds to the control over a large range of forcing Strouhal number and azimuthal modes. Over this range of jet variables, there is a considerable change in the jet acoustic Mach number (0.83 to 2.1) and the theoretical convective Mach number (0.43 to 0.92), a measure of compressibility level. Yet, the jet response, in terms of generating organized flow structures, is similar. The results clearly demonstrate that the jet flow field and acoustic far-field can be dramatically altered, providing a powerful control tool in these practical high-speed and high Reynolds number jets. Sample flow results (phase-averaged Galilean streamlines and Q-criterion) and acoustic results (Mach wave radiation) are presented to demonstrate the capabilities of these actuators and the control technique for flow and acoustic diagnostics.

Acknowledgements

The support of this research by NASA Glenn Research Center with James Bridges and Cliff Brown and by NAVAIR with John Spyropoulos is greatly appreciated. The help and support of Igor Adamovich and discussions with Datta Gaitonde have been instrumental.

References

[1] Samimy, M., Debiasi, M., Caraballo, E., Serrani, A., Yuan, X., Little, J., and Myatt, J.H., "Feedback control of subsonic cavity flows using reduced-order models", *J. Fluid Mech.* Vol. 579, 2007, pp. 315-346.

[2] Sinha, A., Kim, K., Kim, J., Serrani, A., and Samimy, M., "Extremizing Feedback Control of a High-Speed and High Reynolds Number Jet", *AIAA Journal* Vol. 48, No. 2, 2010, pp. 387-399.

[3] Melton, L.P., Schaeffler, N.W., Yao, C.-S., and Seifert, A., "Active Control of Flow Separation from Supercritical Airfoil Leading-Edge Flap Shoulder", *Journal of Aircraft* Vol. 42, No. 5, 2005, pp. 1142-1149.

[4] Little, J., and Samimy, M., "High-Lift Airfoil Separation with Dielectric Barrier Discharge Plasma Actuation", *AIAA Journal* Vol. 48, No. 12, 2010, pp. 2884-2898.

[5] Alkislar, M.B., "Flow Characteristics of a Jet Controlled with Chevron-Microjet Combination for Noise Reduction", AIAA Paper 2009-0851, 2009.

[6] Samimy, M., Kim, J.H., Kastner, J., Adamovich, I., and Utkin, Y., "Active Control of High-Speed and High-Reynolds-Number Jets Using Plasma Actuators", *J. Fluid Mech.* Vol. 578, No. 1, 2007, pp. 305-330.

[7] Moreau, E., "Airflow control by non-thermal plasma actuators", *Journal of Physics D: Applied Physics* Vol. 40, No. 3, 2007, pp. 605-636.

[8] Little, J., Takashima, K., Nishihara, M., Adamovich, I., and Samimy, M., "High Lift Airfoil Leading Edge Separation Control with Nanosecond Pulse Driven DBD Plasma Actuators", AIAA Paper 2010-4256, 2010.

[9] Rethmel, C., Little, J., Takashima, K., Sinha, A., Adamovich, I., and Samimy, M., "Flow Separation Control over an Airfoil with Nanosecond Pulse Driven DBD Plasma Actuators", AIAA Paper, 2011.

[10] Samimy, M., Kim, J.-H., Kearney-Fischer, M., and Sinha, A., "Acoustic and Flow Fields of an Excited High Reynolds Number Axisymmetric Supersonic Jet", *J. Fluid Mech.* Vol. 656, 2010, pp. 507-529.

[11] Michalke, A., and Fuchs, H.V., "On turbulence and noise of an axisymmetric shear flow", *J. Fluid Mech.* Vol. 70, No. 1, 1975, pp. 179-205.

[12] Zaman, K.B.M.Q., and Hussain, A.K.M.F., "Turbulence Suppression in Free Shear Flows by Controlled Excitation", *J. Fluid Mech.* Vol. 103, 1981, pp. 133-159.

[13] Crow, S.C., and Champagne, F.H., "Orderly Structure in Jet Turbulences", *J. Fluid Mech.* Vol. 48, No. 3, 1971, pp. 547-591.

[14] Michalke, A., and Hermann, G., "On the inviscid instability of a circular jet with external flow", *J. Fluid Mech.* Vol. 114, 1982, pp. 343-359.

[15] Cohen, J., and Wygnanski, I., "The evolution of instabilities in the axisymmetric jet. Part 1 the linear growth of disturbances near nozzle", *J. Fluid Mech.* Vol. 176, 1987, pp. 191-219.

[16] Barone, M.F., and Lele, S.K., "Receptivity of the compressible mixing layer", *J. Fluid Mech.* Vol. 540, 2005, pp. 301-335.
[17] Brown, G.L., and Roshko, A., "On density effects and large structure in turbulent mixing layers", *J. Fluid Mech.* Vol. 64, No. 4, 1974, pp. 775-816.
[18] Bechert, D.W., and Pfizenmaier, E., "On the amplification of broad band jet noise by a pure tone excitation", *J. Sound & Vib.* Vol. 43, No. 3, 1975, pp. 581-587.
[19] Moore, C.J., "The role of shear-layer instability waves in jet exhaust noise", *J. Fluid Mech.* Vol. 80, No. 2, 1977, pp. 321-367.
[20] Crighton, D.G., "Jet Noise and the Effects of Jet Forcing", *Lecture Notes in Physics* Vol. 136, 1981, pp. 340-362.
[21] Hussain, A.K.M.F., and Zaman, K.B.M.Q., "The 'preferred mode' of the axisymmetric jet", *J. Fluid Mech.* Vol. 110, 1981, pp. 39-71.
[22] Ahuja, K.K., and Blakney, D.F., "Tone Excited Jets, Part IV: Acoustic Measurements", *J. Sound & Vib.* Vol. 102, No. 1, 1985, pp. 93-117.
[23] Kibens, V., "Discrete Noise Spectrum Generated by an Acoustically Excited Jet", *AIAA Journal* Vol. 18, No. 4, 1980, pp. 434-441.
[24] Hussain, A.K.M.F., and Hasan, M.A.Z., "Turbulence suppression in free turbulent shear flows under controlled excitation. Part 2. Jet-noise reduction", *J. Fluid Mech.* Vol. 150, 1985, pp. 159-168.
[25] Jubelin, B., "New Experimental Studies on Jet Noise Amplification", AIAA Paper 1980-0961, 1980.
[26] Deneuville, P.N., and Jacques, J.R., "Jet Noise Amplification: A Practically Important Problem", AIAA Paper 1977-1368, 1977.
[27] Lu, H.Y., "Effect of Excitation on Coaxial Jet Noise", *AIAA Journal* Vol. 21, No. 2, 1983, pp. 214-220.
[28] Tanna, H.K., and Ahuja, K.K., "Tone Excited Jets. I - Introduction", *J. Sound & Vib.* Vol. 102, No. 1, 1985, pp. 57-61.
[29] Moore, C.J., "The Effect of Shear Layer Instability on Jet Exhaust Noise", *Structure and Mechanisms of Turbulence* Vol. 2, 1977, pp. 254-264.
[30] Heavens, S.N., "Visualization of the acoustic excitation of a subsonic jet", *J. Fluid Mech.* Vol. 100, No. 1, 1980, pp. 185-192.
[31] Zaman, K.B.M.Q., and Hussain, A.K.M.F., "Vortex pairing in a circular jet under controlled excitation. Part 1. General jet response", *J. Fluid Mech.* Vol. 101, No. 3, 1980, pp. 449-491.
[32] Ahuja, K.K., and Whiffen, M.C., "Tone Excited Jets. II - Flow Visualization", *J. Sound & Vib.* Vol. 102, No. 1, 1985, pp. 63-69.
[33] Kusek, S.M., Corke, T.C., and Reisenthel, P., "Seeding of helical modes in the initial region of an axisymmetric jet", *Exp. Fluids* Vol. 10, No. 2-3, 1990, pp. 116-124.
[34] Corke, T.C., and Kusek, S.M., "Resonance in Axisymmetric Jets with Controlled Helical-mode Input", *J. Fluid Mech.* Vol. 249, 1993, pp. 307-336.
[35] Adelgren, R.G., Elliott, G.S., Crawford, J.B., Carter, C.D., Donbar, J.M., and Grosjean, D.F., "Axisymmetric Jet Shear-Layer Excitation by Laser Energy and Electric Arc Discharges", *AIAA Journal* Vol. 43, No. 4, 2005, pp. 776-791.
[36] Hussain, A.K.M.F., "Coherent Structures and Turbulence", *J. Fluid Mech.* Vol. 173, 1986, pp. 303-356.
[37] Chan, Y.Y., "Spatial waves in turbulent jets", *Phys. Fluids* Vol. 17, No. 1, 1974, pp. 46-53.
[38] Morrison, G.L., and McLaughlin, D.K., "Instability Process in Low Reynolds Number Supersonic Jets", *AIAA Journal* Vol. 18, No. 7, 1980, pp. 793-800.
[39] Cohen, J., and Wygnanski, I., "The evolution of instabilities in the axisymmetric jet. Part 2 The Flow resulting from the interaction between two waves", *J. Fluid Mech.* Vol. 176, 1987, pp. 221-235.
[40] Morrison, G.L., and McLaughlin, D.K., "Noise Generation by Instabilities in Low Reynolds Number Supersonic Jets", *J. Sound & Vib.* Vol. 65, No. 2, 1979, pp. 177-191.
[41] Bridges, J., and Hussain, F., "Direct Evaluation of Aeroacoustic Theory in a Jet", *J. Fluid Mech.* Vol. 240, 1992, pp. 469-501.
[42] Lepicovsky, J., Ahuja, K.K., and Salikuddin, M., "An Experimental Study of Tone-Excited Heated Jets", *Journal of Propulsion and Power* Vol. 2, No. 2, 1986, pp. 149-154.
[43] Kibens, V., Dorris, J., III, Smith, D.M., and Mossman, M.F., "Active Flow Control Technology Transition: The Boeing ACE Program", AIAA Paper 1999-3507, 1999.
[44] Ahuja, K.K., Lepicovsky, J., and Burrin, R.H., "Noise and Flow Structure of a Tone-Excited Jet", *AIAA Journal* Vol. 20, No. 12, 1982, pp. 1700-1706.
[45] Lepicovsky, J., and Brown, W.H., "Effects of nozzle exit boundary-layer conditions on excitability of heated free jets", *AIAA Journal* Vol. 27, No. 6, 1989, pp. 712-718.
[46] Low, K., Hadidi, B.E., Andino, M., Berdanier, R., and Glauser, M., "Investigation of Different Active Flow Control Strategies for High Speed Jets Using Synthetic Jet Actuators", AIAA Paper 2010-4267, 2010.
[47] Utkin, Y.G., Keshav, S., Kim, J.-H., Kastner, J., Adamovich, I.V., and Samimy, M., "Development and Use of Localized Arc Filament Plasma Actuators for High-Speed Flow Control", *Journal of Physics D: Applied Physics* Vol. 40, No. 3, 2007, pp. 685-694.
[48] Samimy, M., Adamovich, I., Webb, B., Kastner, J., Hileman, J., Keshav, S., and Palm, P., "Development and characterization of plasma actuators for high-speed jet control", *Exp. Fluids* Vol. 37, No. 4, 2004, pp. 577-588.
[49] Hahn, C., Kearney-Fischer, M., and Samimy, M., "Effects of Ring Groove and Duty Cycle on Plasma Actuator Performance in High Speed Jets", AIAA Paper, 2011.

[50] Kleinman, R.R., Bodony, D.J., and Freund, J.B., "Shear-flow excitation mechanisms of recessed localized arc-filament plasma actuators", *Phys. Fluids* Vol. 22, 2010, pp. 116103.
[51] Kim, J., Nishihara, M., Keshav, S., Adamovich, I., Samimy, M., Gorbatov, S.V., and Pliavaka, F.V., "On the Development of Localized Arc Filament Plasma Actuators for High-Speed Flow Control", AIAA Paper 2009-4071, 2009.
[52] Gaitonde, D., "Simulation of Supersonic Nozzle Flows with Plasma-based Control", AIAA Paper 2009-4187, 2009.
[53] Gaitonde, D.V., and Samimy, M., "Effect of plasma-based azimuthal mode excitation on supersonic jet flow", AIAA Paper 2010-4416, 2010.
[54] Kim, J., Afshari, A., Bodony, D.J., and Freund, J.B., "LES Investigation of a Mach 1.3 Jet With and Without Plasma Actuators", AIAA Paper 2009-0290, 2009.
[55] Kearney-Fischer, M., Kim, J.-H., and Samimy, M., "Control of a high Reynolds number Mach 0.9 heated jet using plasma actuators", *Phys. Fluids* Vol. 21, 2009, pp. 095101.
[56] Kearney-Fischer, M., Kim, J.-H., and Samimy, M., "Flow Control of a High Reynolds Number Mach 1.3 Heated Jet Using Plasma Actuators", AIAA Paper 2010-4418, 2010.
[57] Samimy, M., Kim, J.H., Kastner, J., Adamovich, I., and Utkin, Y., "Active Control of a Mach 0.9 Jet for Noise Mitigation Using Plasma Actuators", *AIAA Journal* Vol. 45, No. 4, 2007, pp. 890-901.
[58] Kim, J.H., Kastner, J., and Samimy, M., "Active Control of a High Reynolds Number Mach 0.9 Axisymmetric Jet", *AIAA Journal* Vol. 47, No. 1, 2009, pp. 116-128.
[59] Kim, J.-H., and Samimy, M., "Effects of Active Control on the Flow Structure in a High Reynolds Number Supersonic Jet", *International Journal of Flow Control* Vol. 1, No. 2, 2009, pp. 99-117.
[60] Kastner, J., Kim, J.-H., and Samimy, M., "A study of the correlation of large-scale structure dynamics and far-field radiated noise in an excited Mach 0.9 jet", *Int. J. Aeroacoustics* Vol. 8, No. 3, 2009, pp. 231-259.
[61] Kearney-Fischer, M., Kim, J.-H., and Samimy, M., "Noise Control of a High Reynolds Number High Speed Heated Jet Using Plasma Actuators", *Int. J. Aeroacoustics* Vol. Accepted 2010, 2011.
[62] Kim, J.-H., Kearney-Fischer, M., Samimy, M., and Gogineni, S., "Far-Field Noise Control in Supersonic Jets From Conical and Contoured Nozzles", *Journal of Engineering for Gas Turbines and Power* Vol. 133, 2011.
[63] Sinha, A., Serrani, A., and Samimy, M., "Initial Development of Reduced-Order Models for Feedback Control of Axisymmetric Jets", *International Journal of Flow Control* Vol. 2, No. 1, 2010, pp. 39-60.
[64] Bechert, D.W., and Stahl, B., "Excitation of Instability Waves in Free Shear Layers. Part 2. Experiments", *J. Fluid Mech.* Vol. 186, 1988, pp. 63-84.
[65] Hunt, J.C.R., WRAY, A.A., and MOIN, P., "Eddies, stream, and convergence zones in turbulent flows": Center for Turbulence Research, 1988, pp. 193.
[66] Jeong, J., and Hussain, F., "On the identification of a vortex", *J. Fluid Mech.* Vol. 285, 1995, pp. 69-94.
[67] Zhou, J., Adrian, R.J., Balachandar, S., and Kendall, T.M., "Mechanisms for generating coherent packets of hairpin vortices in channel flow", *J. Fluid Mech.* Vol. 387, 1999, pp. 353-396.
[68] Adrian, R.J., Christensen, K.T., and Liu, Z.-C., "Analysis and interpretation of instantaneous turbulent velocity fields", *Exp. Fluids* Vol. 29, 2000, pp. 275-290.
[69] Kearney-Fischer, M., Kim, J.-H., and Samimy, M., "A Study of Mach Wave Radiation Using Active Control", *J. Fluid Mech.* Vol. Submitted, 2011.
[70] Samimy, M., Kastner, J., Kim, J.H., Utkin, Y., Adamovich, I., and Brown, C., "Flow and Noise Control in High Speed and High Reynolds Number Jets Using Plasma Actuators", AIAA Paper 2846, 2006.
[71] George, W.K., Beuther, P.D., and Arndt, R.E.A., "Pressure spectra in turbulent free shear flows", *J. Fluid Mech.* Vol. 148, 1984, pp. 155-191.
[72] Arndt, R.E.A., Long, D.F., and Glauser, M.N., "The proper orthogonal decomposition of pressure fluctuations surrounding a turbulent jet", *J. Fluid Mech.* Vol. 340, 1997, pp. 1-33.
[73] Tinney, C.E., Ukeiley, L.S., and Glauser, M.N., "Low-Dimensional Characteristics of a Transonic Jet. Part 2. Estimate and Far-Field Prediction", *J. Fluid Mech.* Vol. 615, 2008, pp. 53-92.
[74] Suzuki, T., and Colonius, T., "Instability waves in a subsonic round jet detected using a near-field phased microphone array", *J. Fluid Mech.* Vol. 565, 2006, pp. 197-226.
[75] Hall, J.W., Pinier, J., Hall, A.e., and Glauser, M., "Two-point correlations of the near and far-field pressure in a transonic jet", ASME Paper FEDSM2006-98458, 2006.
[76] Jordan, P., and Gervais, Y., "Subsonic Jet Aeroacoustics: Associating Experiment, Modelling and Simulation", *Exp. Fluids* Vol. 44, No. 1, 2008, pp. 1-21.
[77] Sinha, A., Serrani, A., and Samimy, M., "Development of Empirical Estimators for Feedback Control of Axisymmetric Jets", AIAA Paper 2010-4419, 2010.